Dielectrophoretic Force Equilibrium of Complex Particles

T. Elkeles,[1] P. García-Sánchez,[2] W. Yue,[1] A. Ramos,[2] and G. Yossifon[1,*]

[1] *Faculty of Mechanical Engineering, Technion—Israel Institute of Technology, Haifa 3200003, Israel*

[2] *Departamento de Electrónica y Electromagnetismo, Facultad de Física, Universidad de Sevilla, Avda. Reina Mercedes s/n, Sevilla 41012, Spain*

(Received 15 May 2020; revised 8 August 2020; accepted 13 October 2020; published 19 November 2020)

In contrast to the commonly used spherical Janus particles, here we use engineered Janus particles that are fabricated by means of the photolithography technique for precise control over their geometry and coated regions. Specifically, we study a "lollipop"-shaped complex particle, the head of which is coated with gold while its tail is left bare. Due to their distinct electrical properties (i.e., electrical polarizability), the particle exhibits force equilibrium, where opposite dielectrophoretic forces acting on its head and tail exactly cancel each other to yield a stable-equilibrium position. This is realized in a quadrupolar electrode array, where the equilibrium position of the engineered particle can be tuned by the frequency. This stands in contrast to the standard dielectrophoretic behavior, where the particle shifts position from either the center of the quad to the very edge of the electrodes when shifting from a negative to positive dielectrophoretic response, respectively. This opens up opportunities for positioning control of such complex particles for self-assembly, biosensing, biomimetic spermatozoa, and more.

DOI: 10.1103/PhysRevApplied.14.054047

I. INTRODUCTION

Dielectrophoresis (DEP), defined as the translational motion of neutral particles due to the effects of polarization in a nonuniform electric field, is a well-established technique that exploits their unique dielectric properties to manipulate particles under alternating current (ac) fields [1]. In particular, a crossover frequency (COF), which is the ac frequency at which the DEP force vanishes, i.e., at which particles shift from attraction to high-field-intensity regions (positive DEP, pDEP) to repulsion (negative DEP, nDEP), can be used as a sensitive discriminator between different particle types or conditions [2,3]. The time-averaged DEP force for a homogeneous dielectric spherical particle suspended within an electrolyte under a nonuniform electric field is represented by $\mathbf{F}_{\mathrm{DEP}} = \pi\varepsilon_e R^3 \mathrm{Re}[\tilde{K}]\nabla|E|^2$, where R is the radius of the particle, E is the amplitude of the electric field, ε_e is the permittivity of the electrolyte, and $\mathrm{Re}[\tilde{K}]$ is the real part of the Clausius-Mossotti (CM) factor [4–6]. The CM factor is defined as $\tilde{K}(\omega) = (\tilde{\varepsilon_p} - \tilde{\varepsilon_e})/(\tilde{\varepsilon_p} + 2\tilde{\varepsilon_e})$, $\tilde{\varepsilon} = \varepsilon + \sigma/(i\omega)$, where $\tilde{\varepsilon_p}$ and $\tilde{\varepsilon_e}$ are the complex permittivities of the particle and the electrolyte, respectively, and ε and σ represent the real permittivity and the conductivity, respectively. The CM depends on the frequency of the electric field, which determines both the direction of the DEP force and its magnitude. The CM factor of micron-size dielectric particles exhibits mostly nDEP, except for dielectric nanoparticles in relatively low-conductivity solutions wherein their surface conductance dominates [7]. In contrast, the CM factor of metallic coated particles has been shown to switch sign from nDEP to pDEP with increasing frequency as the induced electrical double layer (EDL) formed on the metallic coating shifts from full electrical screening to no screening at frequencies sufficiently larger than the *RC* frequency [8–10].

Herein, we exploit this transition of the polarizability of the metallic coating of a complex particle in order to control the interplay between its different coated and noncoated (i.e., dielectric) parts. Such an interplay between the coated and noncoated parts of a particle has been demonstrated for a spherical metallodielectric Janus particle (JP), where its overall DEP and electrorotation (ROT) behavior has been taken to be an average of the same spherical particle as though it was uniformly dielectric and uniformly coated [11]. However, as noted for a certain frequency, the DEP response of the JP was either nDEP or pDEP. Hence, no intermediate equilibrium positions were obtained within the quadrupolar electrode array. In contrast, here we will demonstrate that if we engineer the Janus particle to have a large enough separation between its dielectric and metallic coated parts, similar to sperm cells [12], such intermediate equilibrium positions can be achieved. Such an engineered Janus particle with a controlled geometry and selective metallic coating is obtained using the standard photolithography fabrication technique [13].

*yossifon@tx.technion.ac.il

Janus particles in general represent an emerging field of research that has attracted immense attention in recent years due to their behavior as self-propelling (active) particles. These active particles have found applications in a broad range of areas such as drug delivery, detoxification, environmental remediation, immunosensing, etc. [14]. As opposed to phoretically driven transport, which is characterized by mass migration in response to externally imposed gradients, active particles asymmetrically draw and dissipate energy at the colloidal scale, creating local gradients that drive autonomous propulsion [15]. Since the driving force is produced at the particle level, active colloids are free to travel along individual path lines. In particular, metallodielectric JPs represent a unique subset of active colloids, in which the energy source is an externally applied electric field where the variation of the frequency of applied electric field has been shown to alter both the speed and direction [16–18].

II. EXPERIMENTAL RESULTS

A. Fabrication of particles and experimental details

Particles are fabricated using standard photolithography and metal-deposition techniques, following the protocol described in Ref. [13]. First, SU-8 photoresist (MicroChem, Corp.) is spin coated on a 4-in. silicon (Si) wafer to a thickness of 2 μm and exposed to UV light through a chrome-patterned photomask to form the engineered particles, which are revealed after development of the photoresist. Second, the wafers are spin coated with two layers of NFR-014R photoresist (JSR Micro, Inc.) to reach a thickness of 6 μm and exposed to UV light through an aligned chrome-patterned photomask to form the regions that are exposed to metal deposition via an electron-beam metal evaporator. Instead of mechanical removal of the particles, which can deform them, we introduce an improvement to this technique by depositing a sacrificial layer, such as LOR resist (MicroChem, Corp), prior to that of SU-8 photoresist. Thus, as a last step, the particles are released using Remover PG (MicroChem. Corp).

The chips are fabricated using standard photolithography and consist of either a quadrupolar with a gap of 200 μm and 500 μm for DEP (Fig. 1) and ROT (Fig. 2) characterization, respectively, as well as a ring-electrode array with a gap of 200 μm between the electrodes for control purposes, acting as an electrode geometry in which no stable equilibrium can exist (Fig. 5). The electrolyte solution consists of dissolved KCl salt within deionized water at different concentrations, which is then introduced into a shallow chamber (height of 120 μm) covering the electrode array along with the "lollipop"-shaped particles. In order to reduce adsorption, the chamber is pretreated with 0.2% v/v of Tween 20 (Sigma). The electrodes are connected to a function generator, which we use to control the frequency and amplitude of the applied electric field. For the ROT setup, we use a rotating electric field such that it has a 90° phase shift between the electrodes.

B. Equilibrium positions

A complex particle can be potentially stagnant under the following modes: (1) at the center of the quad under nDEP response [20]; (2) at stable-equilibrium positions within the quad, where the two counteracting DEP forces exactly cancel each other; (3) at the edge of the electrode under pDEP response. This is verified for the lollipop-shaped particle, where the DEP equilibrium (i.e., mode 2) positions are varied with the frequency. Figure 1(a) shows such a complex particle in stable-equilibrium mode, when the frequency of the alternating current electric field is such that parts 1 and 2 of the particles [as defined in Fig. 1(b)] are experiencing DEP forces of comparable magnitude and opposite directions. In order to measure the stable-equilibrium position of the particles, they are placed inside the quad while experiencing an electric field at a specific frequency. Figure 1(c) shows the average equilibrium position of between three and five particles versus the frequency of the applied field. In order to assure that this is indeed a stable-equilibrium position, the particles are often shaken, after which they recover their equilibrium position. In addition, frequencies are applied in a different order to negate the existence of system hysteresis (see Supplemental Video 1 [19]).

It is found that increasing the conductivity of the medium results in a wider range of these equilibrium-frequency windows. In addition, we find that the frequencies at which the particle transitions from nDEP to stable equilibrium and from stable equilibrium to pDEP strongly depend on the solution conductivity and shift to higher values with increasing solution conductivity. Whereas the dielectric (SU8) tail of the particle always exhibits nDEP behavior, the metallic coated head of the particle switches from nDEP to pDEP behavior with increasing frequency at a transition frequency that corresponds to the RC time of the induced EDL. This can explain the shift of the above transitions that is observed for the complex particle as the RC frequency increases linearly with σ_e.

C. Determination of the specific capacitance of the electrical double layer

In order to match the experimental results to the numerical simulations in Sec. II B, the angular frequency must be normalized by the conductivity and the specific capacitance of the electric double layer, C_{DL}, on the metallic coated disk. We conduct several experiments using an electrorotating field (ROT), from which we extract C_{DL}. Due to the relatively high voltage applied on the particle, which exceeds the thermal potential, the linear Debye-Huckel model for the capacitance is not applicable. Furthermore, there is always the ambiguity regarding the Stern-layer

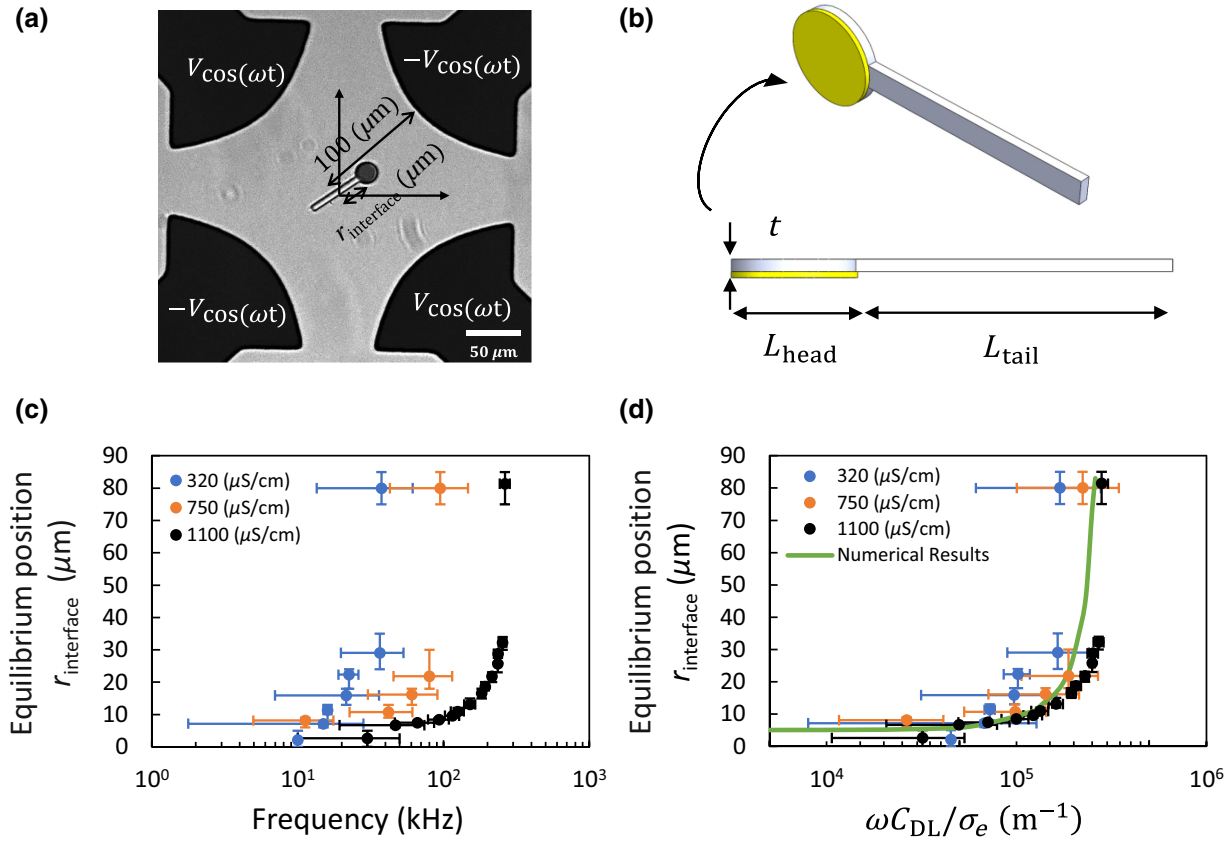

FIG. 1. (a) A microscope image of the complex particle within a quadrupolar electrode array. Here, we define the equilibrium position $r_{\text{interface}}$ from the center of the quad to the interface of the tail and the head of the particle. (b) A schematic of the complex particle with dimensions $L_{\text{tail}} = 50$ μm, $L_{\text{head}} = 20$ μm, $t = 2$ μm, while the thickness of the gold coating is 30 nm, on top of a 10-nm Cr coating (marked with yellow in the scheme). (c) The equilibrium position of the hybrid particle as a function of the electric field frequency. The graph depicts three different electrolyte conductivities at a voltage of either 15 V or 20 V, with no observable difference in the equilibrium position for these two voltages. The error bars represent the standard deviation of several (between three and five) experiments (see Supplemental Video 1 [19]). (d) The experimental and numerical results of the particle position as a function of the normalized frequency.

capacitance, which needs to be resolved somehow. Therefore, the value of C_{DL} is experimentally extracted for each solution conductivity only for the coated-disk particle without the tail section. A rotating electric field is applied in the 500 μm quadrupolar electrode array and the angular velocity of the gold-coated disk is measured in different frequencies [21]. After obtaining the ROT spectra for each conductivity [Fig. 2(a)], we use C_{DL} as a fitting parameter in the normalized experimental curves to match the normalized angular velocities of the point of maximum angular velocity to that obtained in the numerical simulation described in Appendix B [Fig. 2(d)]. Table I shows C_{DL} for the three conductivities.

III. THEORETICAL ANALYSIS AND COMPARISON WITH EXPERIMENTS

A. Heuristic model for the stable equilibrium

The two main parts of the particle are its "head" (1) and the "tail" (2) as described in Fig. 1(b). For a hyperbolic polynomial electrode geometry of $xy = l^2/8$, where l is the electrode spacing [e.g., 200 μm in Fig. 1(a)], the electric field distribution [22] is $|E| = (4\Delta V/l^2)r$ and, accordingly, $\nabla|E|^2 = (32\Delta V/l^2)^2 r\hat{\mathbf{r}}$, where r is the radial coordinate from the center of the quad to the interface between the head and tail of the particle [see Fig. 1(a)]. If we approximate our electrode geometry to be close enough to the hyperbolic polynomial, we can write the nDEP force acting on the center, $r_{\text{tail}} = r_{\text{interface}} - L_{\text{tail}}/2$, of the dielectric tail as

$$\mathbf{f}_{\text{tail}} = -|\alpha_{\text{tail}}| r_{\text{tail}} \hat{\mathbf{r}} \tag{1}$$

and the pDEP force acting on the center, $r_{\text{head}} = r_{\text{tail}} + d = r_{\text{tail}} + (L_{\text{tail}} + L_{\text{head}})/2$, of the coated head as

$$\mathbf{f}_{\text{head}} = \text{Re}[\alpha_{\text{head}}](r_{\text{tail}} + d)\hat{\mathbf{r}}, \tag{2}$$

where d is the distance between the centers of the head and tail of the particle and α_{tail} and α_{head} are

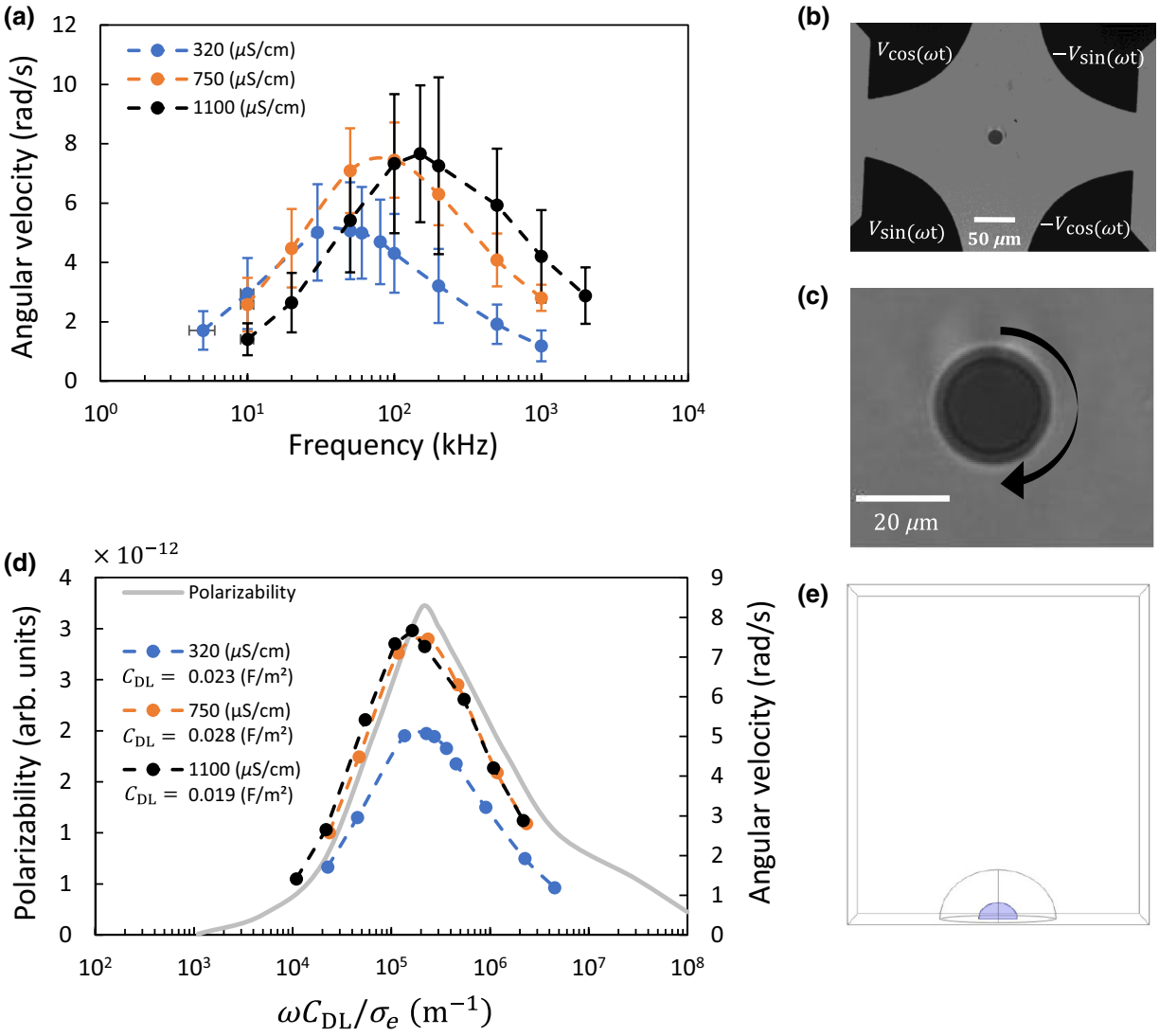

FIG. 2. (a) The ROT velocity of the Au-coated disk (only the "head" part of the complex particle) as a function of the frequency at a voltage of 20 V. The error bars represent the standard deviation of four or five experiments. (b),(c) A microscope image (b) of the coated disk and its enlarged image (c) along with the direction of rotation as observed from the inverted microscope (see Supplemental Video 2 [19]). (d) The ROT velocity of a coated disk as a function of the normalized frequency. The graph also shows the polarizability, which is calculated numerically: the extracted C_{DL} values are indicated in the legend. (e) The computational domain of the numerical simulation.

prefactors of the DEP force including the Clausius-Mossotti factor (i.e., particle polarizability relative to that of the medium). While α_{tail} is negative and independent of the field frequency, $\mathrm{Re}[\alpha_{head}]$ is expected to show a transition from a negative to a positive value—the head polarizability can be described according to $\alpha_{head} \propto (i\omega\tau - 1)/(i\omega\tau + 2)$, where τ is the RC time for charging the head EDL. Thus, for a force equilibrium to exist, the applied frequency must be higher than τ^{-1} for the forces $\mathbf{f}_{tail}$ and $\mathbf{f}_{head}$ to be nDEP and pDEP, respectively. For the equilibrium $|\mathbf{f}_{head}| = |\mathbf{f}_{tail}|$, one obtains the equilibrium position

$$r_{tail}^{eq} = \frac{\mathrm{Re}[\alpha_{head}]}{|\alpha_{tail}| - \mathrm{Re}[\alpha_{head}]} d. \tag{3}$$

An immediate outcome of this heuristic model is that for such an equilibrium to exist, there must be a separation distance d between the centers of the two "point" dipoles of the head and tail. In addition, the real part of the head

TABLE I. The frequencies for maximum angular velocity and the estimated values for C_{DL}.

Electrolyte conductivity [μS/cm]	Frequency for maximum ROT (kHz)	C_{DL} (F/m^2)
320	47 ± 5	0.023 ± 0.002
750	90 ± 12	0.028 ± 0.004
1100	190 ± 20	0.019 ± 0.002

polarizability has to be positive but smaller than the polarizability of the dielectric part, i.e., $|\alpha_{tail}| > \mathrm{Re}[\alpha_{head}] > 0$. When $\mathrm{Re}[\alpha_{head}] > |\alpha_{tail}|$, the pDEP force on the coated head becomes dominant and the overall complex particle behavior becomes pDEP. This is expected to occur at a sufficiently high frequency at which the metallic coating is no longer screened by the induced EDL and hence is beyond the *RC* frequency. At the other extreme, at low frequencies, the metallic coating is fully screened by the induced EDL and hence both the tail and the head exhibit a nDEP behavior and hence the overall complex particle behavior is also expected to be nDEP. Hence, it is only for an intermediate window of frequencies that such an equilibrium occurs. It is also clear that the polarizability of the coated head, which is strongly dependent on the frequency, is increasing in magnitude with increasing frequency and that, accordingly, the equilibrium position r_{tail}^{eq} increases. Figure 3 shows the equilibrium position for the case of a spherical head and tail. Thus, the position of the complex particle shifts toward the edge of the electrodes and away from the quad center with increasing frequency, in accordance with the experimental measurements [Fig. 1(c)]. In addition, as seen in Fig. 4(a), this is a *stable* equilibrium, as any perturbation of the particle position around r_{tail}^{eq} results in a force that restores this position. On the other hand, for the ring-electrode array, the complex particle is positioned

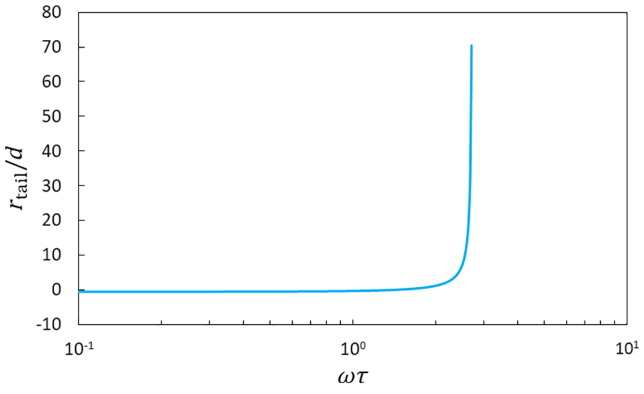

FIG. 3. The equilibrium position of a complex particle as a function of the nondimensional frequency $\omega\tau$. The position is evaluated from Eq. (3) and by considering that the head and tail are spheres with the same radius.

with its head toward and its tail away from the inner ring electrode. Hence, the pDEP force acting on the head of the particle can be written as [23]

$$\mathbf{f}_{head} = -\frac{\mathrm{Re}[\alpha_{head}]}{r_{head}^3}\hat{\mathbf{r}} \tag{4}$$

where r_{head} is the position of the center of the head. The nDEP force acting on the dielectric tail is then

$$\mathbf{f}_{tail} = \frac{|\alpha_{tail}|}{(r_{head}+d)^3}\hat{\mathbf{r}} \tag{5}$$

From Fig. 4(c), it is clear that this equilibrium position is unstable, as any perturbation of the particle position results in its motion toward either the inner or outer ring electrodes depending on its location (or, equivalently, its initial positioning).

B. Numerical results and comparison with experiments

The electrical force on the hybrid lollipop-shaped particle is numerically calculated as a function of the position and frequency. Appendix A contains the details of this calculation. Figure 1(d) shows the particle position within the quadrupolar array at which this force vanishes (i.e., the equilibrium position) as a function of the frequency. Following the extraction of the C_{DL} values (Table I), the experimental results of the equilibrium position are then depicted using a normalized angular frequency and show qualitative agreement with the numerical simulations [Fig. 1(d)]. For simplification, we neglect the contribution of electroconvection induced on the head, as it is expected to be suppressed due to the small gap between its metal face and the bottom of the microchamber (see Supplemental Video 3 [19]).

Figure 4 shows that, for a stable equilibrium to occur, the nonuniform electric field must obey a certain spatial distribution. While the quadrupolar electrode array does satisfy the necessary conditions, other electrode arrays, such as the ring electrode shown in Fig. 5, do not. In accordance with the heuristic model described in the previous section, no such stable equilibrium is experimentally found in such a ring-electrode setup. Instead, it is found that the particles are either repelled from the inner electrode or attracted to it. The results of the simulations suggest that in the ring geometry there exists a range of frequencies for which the particle experiences an unstable equilibrium [Fig. 5(c)]. Depending on the initial radial distance of the particle from the center of the array, the response can be either pDEP or nDEP if it is smaller (i.e., $r_{initial} < r^{eq}$) or larger (i.e., $r_{initial} > r^{eq}$) than the equilibrium position, respectively [Fig. 4(c)]. Hence, due to the unstable equilibrium, there are eventually two terminal positions of the particle, either at the inner electrode edge due to the dominance of pDEP or close to

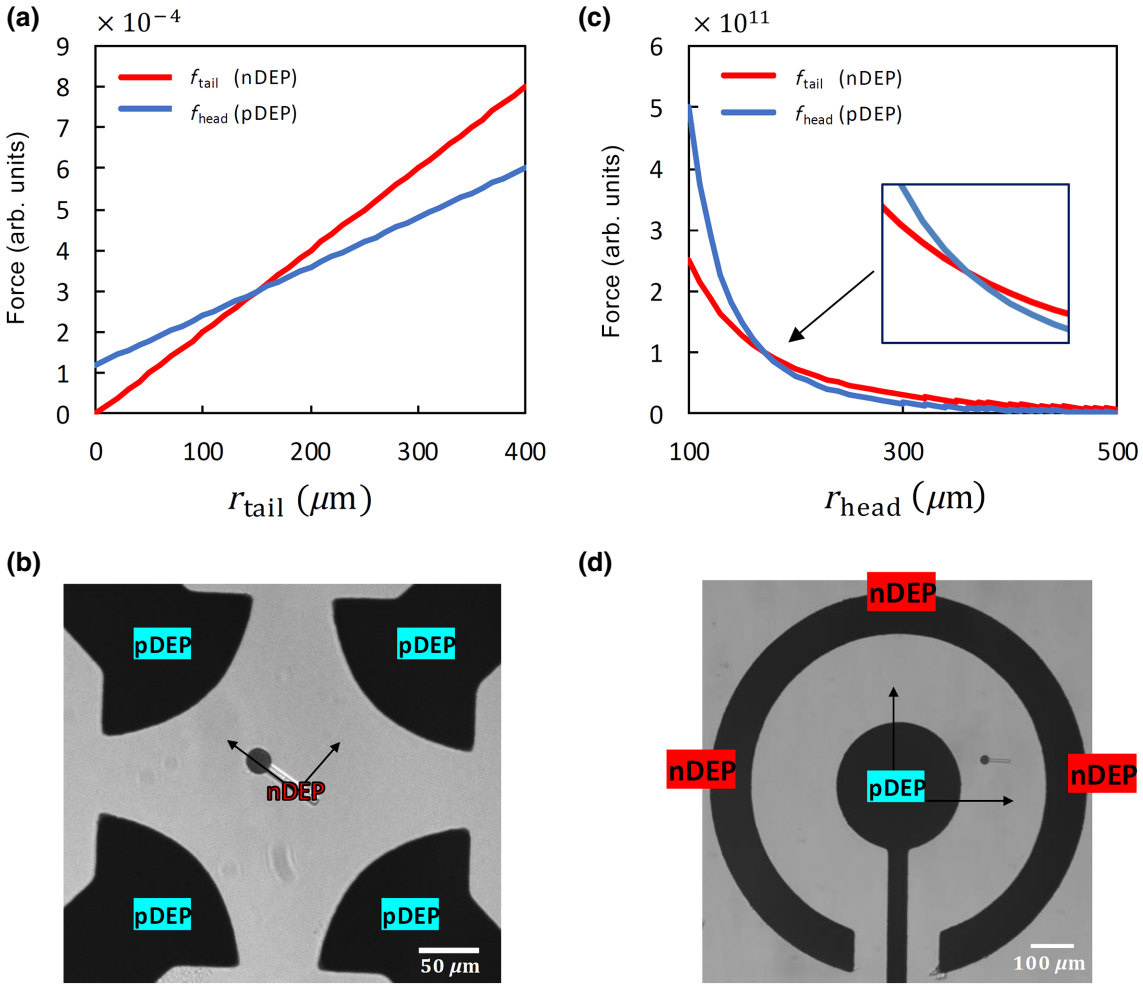

FIG. 4. (a),(b) The absolute force distribution on the head and tail of the particle versus the radial distance of the center of the tail, r_{tail}, from the center of the quadrupolar electrode array yielding a stable equilibrium (see Supplemental Video 1 [19]). (c),(d) The absolute force distribution on the particle versus the radial distance of the center of the head, r_{head}, from the center of the ring-electrode array yielding an unstable equilibrium (see Supplemental Video 4 [19]).

the edge of the outer ring electrode due to the dominance of nDEP. It is worth noting that since our system is not an ideal two-dimensional geometry but is actually three-dimensional (3D) and hence there is an electric field intensification at the very edge of the outer ring electrode, the potential well of the nDEP is somewhat away from the edge of the outer ring electrode (see Supplemental Video 4 [19]).

IV. CONCLUSIONS AND OUTLOOK

We demonstrate that a complex engineered particle, where opposite DEP forces can occur in its different parts, exhibits a stable equilibrium within a frequency range. In addition, we find that the frequencies at which the particle transitions from nDEP to stable equilibrium and from stable equilibrium to pDEP strongly depend on the solution conductivity, as expected. A quantitative comparison between the numerical results of the equilibrium position as a function of the frequency and the experimental results validates this and provides further information on the dependency of the equilibrium range with the solution conductivity. The ROT spectra on the coated disk show that, indeed, the metallic part of the particle undergoes transition from nDEP to pDEP as expected and the frequency of maximum angular velocity increases with increasing conductivity. This ability to control the equilibrium position of complex particles by simply changing the applied electric field frequency may open up opportunities for the self-assembly of complex particles, as they can self-migrate to positions of stable equilibrium. Moreover, if there are many such particles, they can interact with each other while migrating and form an interesting collective behavior (see Supplemental Video 5 [19]). A more controlled interaction is observed for two such complex particles wherein their separation distance of the

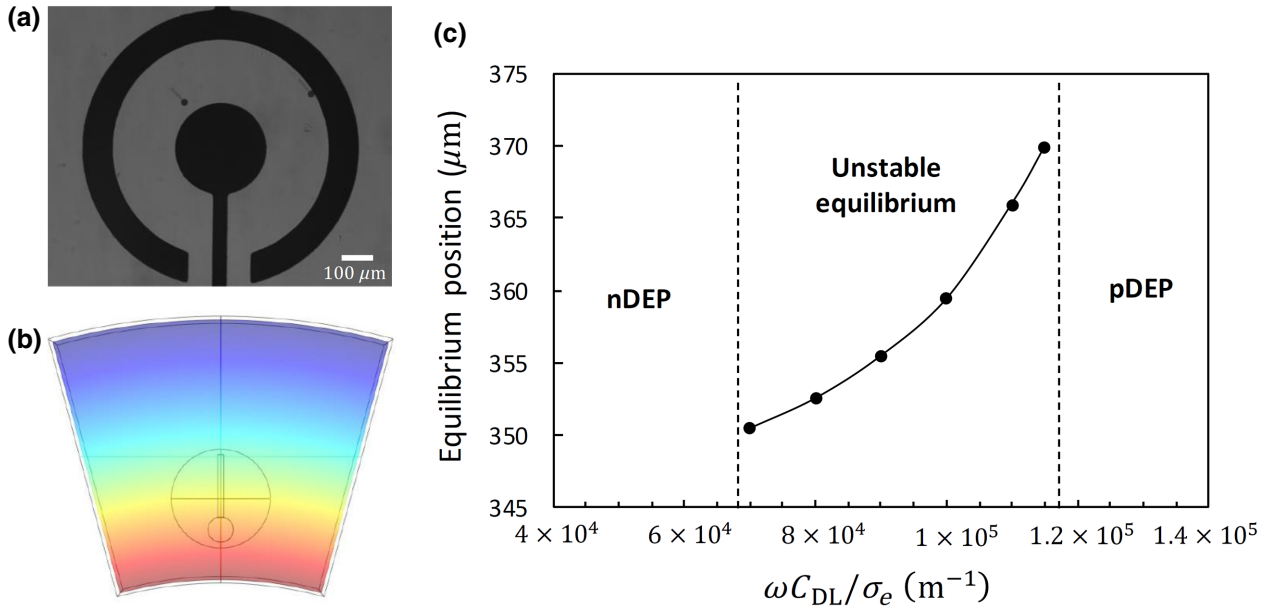

FIG. 5. (a) A microscope image of the complex particle inside the ring-shaped electrode array with a gap of 200 μm gap between the inner and outer electrodes. (b) The computational domain of the numerical simulation with the particle enveloped within a spheroidal surface. The colors denote the magnitude of the electric potential. (c) The numerical-simulation results, indicating that there is an unstable equilibrium in the frequency regime between a nDEP and pDEP response (see Supplemental Video 4 [19]).

equilibrium positions can be sensitively controlled by the frequency (see Fig. 6 and Supplemental Video 6 [19]). The measured distance between the heads [Fig. 6(b)] qualitatively follows the same trend as that of a single complex particle (Fig. 1). However, due to interparticle interaction, it is not simply just a translation from Fig. 1(c). Furthermore, if the metallic coated regions of the particle are functionalized with molecular probes (e.g., antibodies), the polarizability of this region can be changed upon binding to a specific target analyte and, hence, form a biosensor that is detected by the change of the equilibrium position. Such complex particles are also reminiscent of self-propelling biological cells (e.g., sperm cells), in that an understanding of their DEP response can help in manipulation (e.g., sorting, accumulation) of such cells. Such complex particles can be designed to mimic the behavior of sperm cells, with their heads exhibiting a nDEP response while their tails can shift from nDEP to pDEP at frequencies beyond the relaxation time of the induced charge [12]. This is realized for the same complex particle but with a Au coating on its tail. As seen in Supplemental Video 7 [19], such a distinct head-and-tail DEP response can be exploited for manipulating the particle and enabling its trapping as well as translation along the edge of the electrode, reminiscent of the strategy used in Ref. [12] to sort out live sperm cells. Moreover, such complex particles can also behave as synthetic self-propelling (i.e., active) particles, also termed micromotors and, hence, an understanding of their DEP response enables additional control over their motion.

ACKNOWLEDGMENTS

We wish to acknowledge the Technion Russel-Berrie Nanotechnology Institute (RBNI) and the Technion Micro-Nano Fabrication Unit (MNFU) for their technical support. P.G.S. and A.R. acknowledge financial support by the European Regional Development Fund (ERDF) and the Spanish Research Agency MCI under Contract No. PGC2018-099217-B-I00.

T. Elkeles and P. García-Sánchez contributed equally to this work.

APPENDIX A: NUMERICAL CALCULATION OF THE ELECTRICAL FORCE ON THE COMPLEX PARTICLE

The hybrid metallodielectric particle is subjected to an ac electric field with angular frequency ω. Using phasors, the electric field can be written as $\mathbf{E}(\mathbf{r},t) = \mathrm{Re}[\tilde{\mathbf{E}}(\mathbf{r})\exp(i\omega t)]$, where $\tilde{\mathbf{E}}(\mathbf{r})$ is the electric field phasor and i is the imaginary unit. The time-averaged electrical force on the complex particle can be computed as the flux of the time-averaged Maxwell stress tensor over a surface S that encloses the particle:

$$\mathbf{F}_{\mathrm{DEP}} = (1/2)\varepsilon \oint_S \mathrm{Re}[\tilde{\mathbf{E}}\tilde{\mathbf{E}}^* - (1/2)\mathbb{I}(\tilde{\mathbf{E}}\cdot\tilde{\mathbf{E}}^*)]\cdot\mathbf{n}\mathrm{d}S, \quad \text{(A1)}$$

where * indicates the complex conjugate, ε is the dielectric constant of the electrolyte, $\mathbb{I}$ is the identity matrix, and $\mathbf{n}$ is a vector normal to the integration surface S.

Thus, prior to the evaluation of Eq. (A1), we have to find the electric field from the solution of the electric potential, ϕ, in the 3D domain of Fig. 7(a). For simplicity, we consider vertical electrodes with a hyperbolic shape instead of the circular coplanar electrodes used in the experiments. Both configurations of electrodes generate a similar electric field structure—differences only appear in a region close to the electrode edges. We use COMSOL to solve the Laplace equation ($\nabla^2\tilde{\phi} = 0$) subject to the following conditions:

(a) Pairs of facing electrodes are subjected to -1 V and 1 V, respectively.

(b) The particle tail is insulating. Thus, zero normal current is imposed on its surface: $(\partial\tilde{\phi}/\partial n) = 0$.

(c) The particle head has a cylindrical shape, with one of its bases coated with a gold layer and facing the electrode substrate. The applied electric field induces an electrical double layer (EDL) at the metal-electrolyte interface. The charging of this EDL is modeled by the following boundary condition [24]:

$$\sigma_e(\partial\tilde{\phi}/\partial n) = i\omega C_{\mathrm{DL}}(\tilde{\phi} - \tilde{V}_{\mathrm{metal}}), \tag{A2}$$

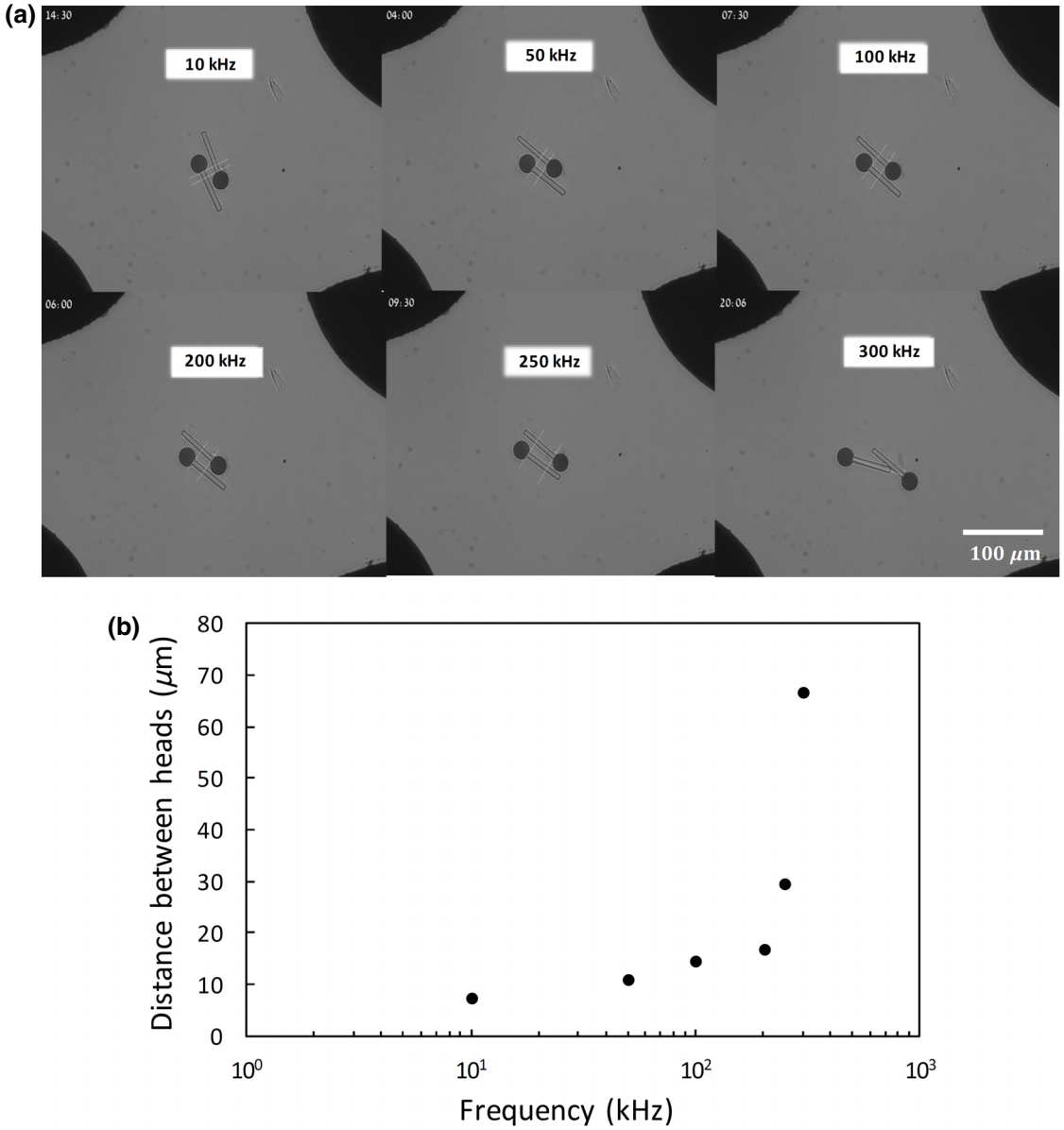

FIG. 6. (a) A microscope image of an assembly of two complex particles within a quadrupolar electrode array. As can clearly be seen, the separation distance between the two particles is controlled by the applied frequency. (b) The experimental results of the separation distance between the two particles as a function of the normalized frequency.

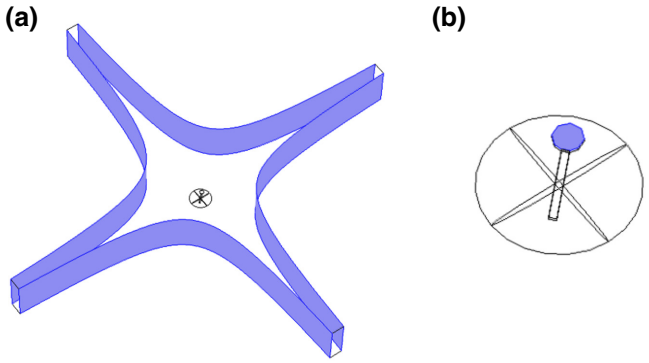

FIG. 7. (a) The computational domain of the numerical simulation, showing the quadrupolar electrodes as well as the complex particle. (b) An enlarged image of the complex particle enveloped within an ellipsoidal surface at which the Maxwell-stress integration is performed in determining the DEP force.

where σ_e is the electrolyte conductivity, C_{DL} is the surface capacitance of the metal-electrolyte interface, and $\tilde{V}_{\mathrm{metal}}$ is the electric potential of the metal layer.

(d) $\tilde{V}_{\mathrm{metal}}$ is an unknown, which is determined after imposing the condition that the total current on the head surface must be zero, i.e., the gold layer acts as a floating electrode with potential $\tilde{V}_{\mathrm{metal}}$. We include an additional integral equation in COMSOL to ensure this condition.

The lollipop-shaped particle is enclosed by an ellipsoid (see Fig. 7). We use this smoother surface for two purposes: (1) to evaluate the integral equation that determines $\tilde{V}_{\mathrm{metal}}$ by imposing zero current on the head surface, and (2) to integrate the Maxwell stress tensor given in Eq. (A1).

APPENDIX B: POLARIZABILITY OF THE DISK AND DOUBLE-LAYER CAPACITANCE

One important parameter in our system is the surface capacitance (C_{DL}) of the EDL induced at the metal-electrolyte interface. In order to determine this parameter, we measure the electrorotation spectrum of the lollipop head: a single disk with one side coated with gold. To this end, we generate a rotating electric field using the 500-μm-gap quadrupolar array. Microelectrodes are subjected to ac signals of angular frequency ω and amplitude V_0. The phase-lag between neighboring electrodes is fixed to 90° [see Fig. 2(b)]. We observe that the disk rotates in the opposite direction to the field rotation, i.e., counterfield rotation. Figure 2(a) shows the measurements of the angular velocity as a function of the frequency for a voltage amplitude of 20 V and three different conductivities. The frequency for maximum angular velocity depends on the conductivity of the electrolyte.

Theoretically, the angular velocity of the particle is calculated by balancing the time average of the electrical torque on the particle and the viscous torque. The electric dipole induced on the particle is written as $\mathbf{p} = \mathrm{Re}[\tilde{\mathbf{p}}(\omega)\exp(i\omega t)]$, where $\tilde{\mathbf{p}}(\omega)$ is the induced dipole phasor. The time average of the electrical torque is calculated as $\boldsymbol{\tau}_E = (1/2)\mathrm{Re}[\tilde{\mathbf{p}} \times \tilde{\mathbf{E}}^*]$, where $\tilde{\mathbf{E}}$ is the electric field phasor. For an electric field rotating clockwise within the X-Y plane, $\tilde{\mathbf{E}} = E_0(\hat{\mathbf{x}} + i\hat{\mathbf{y}})$. The induced dipole can be written as $\tilde{\mathbf{p}}(\omega) = 4\pi\varepsilon\tilde{A}(\omega)\tilde{\mathbf{E}}$ and the time-averaged torque is:

$$\boldsymbol{\tau}_E = 4\pi\varepsilon E_0^2 \mathrm{Im}[\tilde{A}]\hat{\mathbf{z}}. \tag{B1}$$

The viscous torque on a disk rotating around its axis can be written as $\boldsymbol{\tau}_v = -k\dot{\theta}\hat{\mathbf{z}}$, where $\dot{\theta}$ is the angular velocity and k is a friction coefficient. The steady-state angular velocity is then given by

$$\dot{\theta} = \frac{4\pi\varepsilon E_0^2}{k}\mathrm{Im}[\tilde{A}]. \tag{B2}$$

Thus, the frequency dispersion of the electrorotation curve is given by the imaginary part of the particle polarizability.

1. Particle polarizability

The particle polarizability can be found from the solution of the electric potential for a particle subjected to a homogeneous electric field with a fixed direction. Let us assume that the disk is subjected to an electric field along an axis parallel to a disk diameter, such as $\tilde{\mathbf{E}} = E_0\hat{\mathbf{x}}$ or, equivalently, an applied electric potential $\tilde{\phi} = -E_0 x$. The electric potential within the electrolyte is a solution of the Laplace equation ($\nabla^2\tilde{\phi} = 0$), with boundary conditions on the disk surface as in the previous section [$\partial\tilde{\phi}/\partial n = 0$ on insulating surfaces and $\partial\tilde{\phi}/\partial n = i\Omega(\tilde{\phi} - \tilde{V}_0)$ on the metallic face].

The perturbation of the electric potential due to the disk is $\tilde{\phi}' = \tilde{\phi} + E_0 x$. $A(\Omega)$ can be computed by projecting $\tilde{\phi}'$ on the Legendre polynomial of order one [25,26]:

$$A(\Omega) = \frac{3}{4\pi E_0}\int_S (\tilde{\phi} + E_0 x)\mathrm{P}_1(\cos\theta)\mathrm{d}S, \tag{B3}$$

where the integration is performed over a surface S that encloses the disk and $\mathrm{P}_1(\cos\theta) = \cos\theta$.

We use COMSOL to compute the polarizability of the disk along an axis parallel to a diameter. For similarity with experiments, we consider a disk with its metal side facing a wall at a distance of approximately 1 μm. Figure 8 shows the imaginary part of $\tilde{A}$ as a function of Ω. Importantly for our purposes, a maximum of $\mathrm{Im}[\tilde{A}]$ occurs for $\Omega \approx 2.1 \times 10^5\ \mathrm{m}^{-1}$.

2. Double-layer capacitance

According to Fig. 8, the double-layer capacitance can be inferred as $C_{\mathrm{DL}} = 2.1 \times 10^5\sigma_e/(2\pi f_{\mathrm{max}})$, where f_{max} is the frequency for peak electrorotation in experiments. We

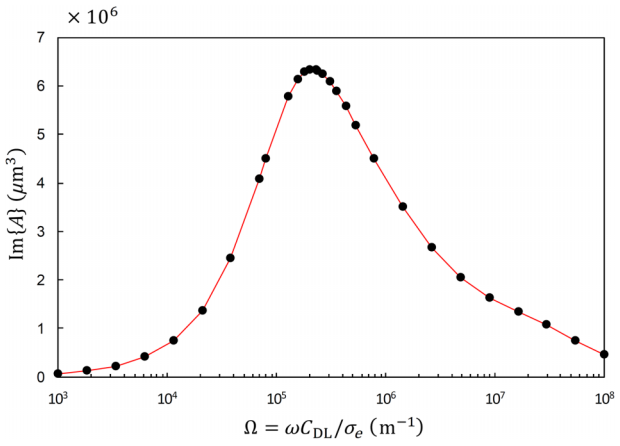

FIG. 8. The imaginary part of the particle polarizability as a function of $\Omega = \omega C_{\mathrm{DL}}/\sigma_e$.

determine $f_{\max}$ by fitting the data to a Lorentzian curve, $Ax/[1 + (x/f_{\max})^2]$. Table I shows the results for the three different conductivities.

[1] T. B. Jones, Liquid dielectrophoresis on the microscale, J. Electrostat. **51**, 290 (2001).

[2] D. Ben-Bassat, A. Boymelgreen, and G. Yossifon, The influence of flow intensity and field frequency on continuous-flow dielectrophoretic trapping, J. Colloid Interface Sci. **442**, 154 (2015).

[3] H. Zhang and M. Chiao, Anti-fouling coatings of poly(dimethylsiloxane) devices for biological and biomedical applications, J. Med. Biol. Eng. **35**, 143 (2015).

[4] H. Morgan and N. G. Green, *AC Electrokinetics: Colloids and Nanoparticles* (Research Studies Press, Hertfordshire, United Kingdom, 2003).

[5] Z. R. Gagnon, Cellular dielectrophoresis: Applications to the characterization, manipulation, separation and patterning of cells, Electrophoresis **32**, 2466 (2011).

[6] T. B. Jones, Basic theory of dielectrophoresis and electrorotation, IEEE Eng. Med. Biol. Mag. **22**, 33 (2003).

[7] C. T. O'Konski, Electric properties of macromolecules. V. Theory of ionic polarization in polyelectrolytes, J. Phys. Chem. **64**, 605 (1960).

[8] P. García-Sánchez, Y. Ren, J. J. Arcenegui, H. Morgan, and A. Ramos, Alternating current electrokinetic properties of gold-coated microspheres, Langmuir **28**, 13861 (2012).

[9] J. J. Arcenegui, P. García-Sánchez, H. Morgan, and A. Ramos, Electro-orientation and electrorotation of metal nanowires, Phys. Rev. E **88**, 063018 (2013).

[10] J. J. Arcenegui, P. García-Sánchez, H. Morgan, and A. Ramos, Electro-orientation of a metal nanowire counterbalanced by thermal torques, Phys. Rev. E **89**, 062306 (2014).

[11] Y.-L. Chen and H.-R. Jiang, Electrorotation of a metallic coated Janus particle under ac electric fields, Appl. Phys. Lett. **109**, 191605 (2016).

[12] S. Shuchat, S. Park, S. Kol, and G. Yossifon, Distinct and independent dielectrophoretic behavior of the head and tail of sperm and its potential for the safe sorting and isolation of rare spermatozoa, Electrophoresis **40**, 1606 (2019).

[13] C. W. Shields IV, K. Han, F. Ma, T. Miloh, G. Yossifon, and O. D. Velev, Supercolloidal spinners: Complex active particles for electrically powered and switchable rotation, Adv. Funct. Mater. **28**, 1803465 (2018).

[14] B. Kherzi and M. Pumera, Self-propelled autonomous nanomotors meet microfluidics, Nanoscale **8**, 17415 (2016).

[15] K. Han, C. W. Shields IV, and O. D. Velev, Engineering of self-propelling microbots and microdevices powered by magnetic and electric fields, Adv. Funct. Mater. **28**, 1705953 (2018).

[16] J. Yan, M. Han, J. Zhang, C. Xu, E. Luijten, and S. Granick, Reconfiguring active particles by electrostatic imbalance, Nat. Mater. **15**, 1095 (2016).

[17] A. Boymelgreen, G. Yossifon, and T. Miloh, Propulsion of active colloids by self-induced field gradients, Langmuir **32**, 9540 (2016).

[18] T. M. Squires and M. Z. Bazant, Breaking symmetries in induced-charge electro-osmosis and electrophoresis, J. Fluid. Mech. **560**, 65 (2006).

[19] See Supplemental Material at http://link.aps.org/supplemental/10.1103/PhysRevApplied.14.054047 for Supplemental Videos 1–7.

[20] J. Voldman, R. A. Braff, M. Toner, M. L. Gray, and M. A. Schmidt, Holding forces of single-particle dielectrophoretic traps, Biophys. J. **80**, 531 (2001).

[21] S. Park, D. Capelin, G. Piriatinskiy, T. Lotan, and G. Yossifon, Dielectrophoretic characterization and isolation of jellyfish stinging capsules, Electrophoresis **38**, 1996 (2017).

[22] Y. Huang and R. Pethig, Electrode design for negative dielectrophoresis, Meas. Sci. Technol. **2**, 1142 (1991).

[23] D. L. Fan, F. Q. Zhu, R. C. Cammarata, and C. L. Chien, Manipulation of nanowires in suspension by ac electric fields, Appl. Phys. Lett. **85**, 4175 (2004).

[24] A. Ramos, H. Morgan, N. G. Green, and A. Castellanos, Ac electric-field-induced fluid flow in microelectrodes, J. Colloid Interface Sci. **217**, 420 (1999).

[25] T. B. Jones, *Electromechanics of Particles* (Cambridge University Press, Cambridge, United Kingdom, 1995).

[26] J. J. Arcenegui, P. García-Sánchez, H. Morgan, and A. Ramos, Electric-field-induced rotation of Brownian metal nanowires, Phys. Rev. E **88**, 033025 (2013).